Reversed double-beam photoacoustic spectroscopy of metal-oxide powders for estimation of their energy-resolved distribution of electron traps and electronic-band structure

Akio Nitta,[1] Mai Takashima,*[1,2] Naoya Murakami,[3] Mai Takase,[4] Bunsho Ohtani[1,2]

[1]Graduate School of Environmental Science, Hokkaido University, Sapporo 060-0810, Japan
[2]Institute for Catalysis, Hokkaido University, Sapporo 001-0021, Japan
[3]Graduate School of Life Science and Systems Engineering, Kyushu Institute of Technology, Kitakyushu 808-0196, Japan
[4]Graduate School of Engineering, Muroran Institute of Technology, Muroran 050-8585, Japan

Keywords reversed double-beam photoacoustic spectroscopy, energy-resolved distribution of electron traps, valence band-top position, metal-oxide powders

ABSTRACT

A novel instrumental methodology, reversed double-beam photoacoustic spectroscopy (RDB-PAS), was developed for measuring the energy-resolved distribution of electron traps (ERDT) of metal-oxide powders. In the RDB-PAS measurement, electrons in the valence band of a powder sample are directly excited to electron traps (ETs) and accumulated in the ETs from the deeper (anodic) side to the shallower (cathodic) side by wavelength-scanned continuous light, and the increase in photoabsorption of electron-filled ETs is measured by modulated light at a fixed wavelength by PAS. It was shown that ERDT/CBB (conduction-band bottom) patterns measured by RDB-PAS can be used for not only identification and detailed characterization of a wide range of metal-oxide powder samples but also estimation of difference in apparent valence-band top (VBT) position.

1. Introduction

One of the hidden, i.e., unrecognized, problems prohibiting sound progress or a breakthrough in the field of electrochemistry is that solid materials used in electrochemical studies have never been identified in the strict scientific sense, i.e., those materials are characterized only by their bulk-structural properties. This is highly contrastive to studies using molecular or metal-complex materials, in which the materials have been almost completely identified, i.e., they have been correctly named according to the nomenclature of chemical substances. The difficulty in identification of solid electrochemical materials is

*corresponding author.
E-mail address: takashima.m@cat.hokudai.ac.jp (Mai Takashima)

simply that they have surfaces and there are no analytical methods to characterize surface structures in macroscopic, not microscopic, ways. Electrochemistry is, in the most comprehensive definition, chemistry in charge transfer through an interface between different phases, especially a solid-liquid interface in ordinary electrochemical systems. In other words, charges e.g., electrons, are transferred through the surfaces of solid materials which have not been identified (not fully characterized) in conventional electrochemical studies; virtual "surface states" have been conveniently used, if necessary, to explain surface-related issues. It is therefore necessary to develop a macroscopic method for characterization of the surfaces of solid electrochemical materials.

Metal oxides have been used and will continue to be used for various purposes such as photocatalysts, catalysts, sensors and luminescence materials. Many of the electrodes used in electrochemical studies are composed of metal oxides, e.g., dye-sensitized solar cells have porous layers containing titania (or another metal oxide) as electrodes, and it is well known that the surfaces of metal electrodes are more or less covered with oxides unless those oxide layers are removed intentionally. In general, metal oxides are categorized as semiconductors or insulators according to their electronic energy structure, i.e., a band structure composed of an electron-filled valence band (VB), electron-vacant conduction band (CB) and forbidden band (bandgap) separating them from each other [1]. Since oxygen anions (O^{2-}s) in the metal-oxide crystalline bulk tend to be detached, more easily than are metal cations, to leave electrons in an oxygen defect, almost all of the semiconducting metal oxides are believed to be n-type semiconductors that have electron-filled donor levels below the CB bottom (CBB). If those donor electrons flow out to reduce, e.g., water or surface hydroxyl groups, those donor levels are left vacant and can be electron traps (ETs). On the other hand, it is well known that color change is induced by calcination of metal-oxide powders under a hydrogen atmosphere or in vacuum, by photoirradiation of suspended metal-oxide powders in the presence of electron donors under deaerated conditions or by cathodic reduction of particulate metal-oxide electrodes. For example, titanium(IV) oxide (titania) and tungsten(VI) oxide turn gray and blue, respectively, and those colorations are attributed to reduced (electron-accepted) titanium ions (Ti^{3+}) [2-7] and tungsten(V) ions [8] accompanied by proton insertion (These reactions are surely electrochemical processes, i.e., charge transfer through interfaces, though this system does not contain electrodes.). For titania powders, the molar amount of accumulated Ti^{3+}s in titania particles in photoirradiated suspensions containing electron donors [9], measured by chemical titration with methyl viologen (MV^{2+}), was saturated and the saturation limits were different depending on the kind of titania samples. In other words, metal-oxide powders such as titania have vacant (empty) electronic levels, ETs, in/on them. A paper [10] from the laboratory of present authors and the above-cited papers [4-6] suggested that ETs were predominantly located on the surfaces of metal oxides.

ET densities in metal oxides have been analyzed by various methods. In recent studies [11,12], surface ET density was estimated by diffuse-reflectance infrared Fourier transform (DRIFT) analysis of nitrobenzene adsorbed onto anatase and rutile titania powders, assuming that surface ET density is equal to twice the molar amount of adsorbed nitrobenzene. Total ET density in titania samples has been estimated in a more direct manner by measurement of accumulated electrons using the above-mentioned photochemical (PC) method [9]. In PC analysis, titania suspensions were photoirradiated by UV light in the presence of electron donors for a period of up to several days in order to fill all of the ETs with electrons, and MV^{2+} was injected to make the trapped electrons reduce MV^{2+} to methyl viologen cation radical ($MV^{\bullet+}$). Then molar amount of $MV^{\bullet+}$ was measured by photoabsorption spectroscopy. Thus, total ET density can be quantitatively measured using chemical titration methods.

However, results for analysis of the energy-resolved distribution of ETs (ERDT) of metal-oxide powders have only been shown in a few papers. In the field of semiconductor physics, for energy-resolved measurement of the density of crystalline defects, which are ETs, in semiconductor materials, thermally stimulated capacitance and current methods were used in the past and deep-level transient spectroscopy (DLTS) with higher sensitivity is now frequently used [13]. An example of metal-oxide ERDT measurements by DLTS is measurements for epitaxially grown MOCVD (metal organic chemical vapor deposition) anatase films [14,15]. The reported ET densities were 0.0025 and 0.027 μmol g^{-1} (data converted assuming the density of an anatase crystal to be 4 g cm^{-3}) at 0.12 eV and 0.96 eV from the CBB, respectively. These densities are much lower than the total ET density, ten to several tens of μmol g^{-1}, in titania powders measured by chemical titration methods, suggesting that deep traps are detected by DLTS only in the bulk of samples.

One of the successful methods for ERDT analysis is the above-mentioned PC method. For ERDT measurements, MV^{2+} was added by changing the pH of photoirradiated titania suspensions from low pH to high pH. As is well known, since band positions, as well as ET levels, of metal oxides are shifted depending on pH of the electrolyte solution, ET energy can be increased with an increase in pH by ca. 60 mV per decade, while electrode potential of an $MV^{2+}/MV^{\bullet+}$ redox couple is constant, not depending on pH. As is discussed in **Results and Discussion**, the observed ERDT of titania samples may be, to the authors' knowledge, the only example of ERDT analysis of metal-oxide samples in the form of powder. However, this PC method requires a very careful operation to avoid leakage of oxygen from the atmosphere, and the measurable energy range and energy resolution, governed by the accuracy in pH control, have been limited and poor, respectively. A spectroelectrochemical method using electrodes prepared from powder samples set in a diffuse-reflectance spectrometer [16] was reported for determination of the ERDT of titania samples and it seems to be better than the PC method, especially in the possible energy range

and resolution. However, the electrode preparation process might change the surface structure of samples, resulting in a change in ERDT, and there seems to be no guarantee that all of the particles in the electrodes participate in the electrochemical process. Thus, a new ERDT analysis methodology using powder samples without changing their form is highly desirable.

Here, a new technique for measurement of the ERDT of metal-oxide samples in their powder form is reported. The principle is (i) accumulation of electrons in ETs from the deeper (anodic) side to the shallower (cathodic) side by direct photoexcitation of electrons from the VB to ETs by wavelength-scanned continuous monochromatic light and (ii) photoacoustic (PA) detection of the photoabsorption of accumulated electrons in ETs by modulated 625-nm light, enabling ERDT measurement for the metal-oxide samples in their powder form. The PA effect, generation of sound by a light-absorbing sample under intermittent light irradiation, was discovered by Bell, the inventor of the telephone, in 1880 [17]. Although, at first, PA spectroscopy (PAS) was used only for gaseous samples, a theory of solid PA effects was established in 1976 [18] and thereafter PAS has been widely used for solid samples. Under intermittent light irradiation, if a sample, in any form (gas, liquid or solid), absorbs the light, electronic, vibrational or rotational excitation occurs and at least a part of those excited states is deactivated to release heat, which expands the volume of a sample, and the expanded sample is shrunk at the interval of photoabsorption. Be repeating the expansion-shrinking cycles under intermittent light irradiation, sound with a frequency that is the same as that of the intermittent light is created. In ordinary photoabsorption spectroscopy, in which reduction (extinction) of light intensity due to photoabsorption of samples is measured, the influence of extinction other than photoabsorption, such as scattering or diffuse reflection, cannot be excluded and a detector that can measure the intensity of irradiated light is necessary. On the other hand, the PA signal reflects only photoabsorption, and a microphone, which does not depend on the wavelength of irradiated light, can be used. Therefore, PAS is one of the best techniques for measurement of the photoabsorption of powder samples, though PA signal intensity means only the relative degree of photoabsorption and calibration is therefore always necessary.

Inspired by the successful application of PAS to semiconducting metal-oxide powder samples reported by Toyoda [19-21], double-beam photoacoustic spectroscopy (DB-PAS) was developed for analysis of the photoinduced change of photocatalysts themselves under conditions similar to those in real applications of photocatalysis [22-24]. It was shown that continuous light does not have any effects on PA signal detection, and it was therefore possible to detect photoabsorption of a sample at the wavelength of continuous light irradiation in DB-PAS. One of the successful results of DB-PAS was analysis of ET filling by bandgap excitation of titania photocatalysts; spectra of electron-filled ETs were obtained and total density of ETs in the titania samples were determined [24].

In order to measure ERDT of metal-oxide powders, reversed double-beam photoacoustic spectroscopy (RDB-PAS) has been developed by modifying DB-PAS. In RDB-PAS, the mode of wavelength scanning is reversed; continuous light driving a photoreaction is wavelength-scanned (fixed wavelength in DB-PAS) and modulated (chopped) light generating the PA signal is wavelength-fixed (wavelength scanned in DB-PAS) [25]. In this paper, principle, the measurement setups, procedure and results of RDB-PAS are reported, and the thus-obtained ERDT patterns of metal-oxide samples are discussed.

2. Experimental

2.1 Materials

Commercial products and Japan Reference Catalyst (JRC) samples of titania provided by the Catalysis Society of Japan (TIO series) were used. The procedure for characterization of the powder samples has been reported elsewhere [25-27]. For ca. 50 titania samples, structural characteristics and some of the results of RDB-PAS analysis are summarized in **Table 1**.

(**Table 1** Structural and ET-related properties and photocatalytic-activity rank of titania samples used in this study)

For preparation of a mixture of JRC-TIO-1 and TIO-3 powder samples, samples of equal weights were put in an agate mortar, mixed thoroughly with a Teflon spatula, and brayed manually for 10 min.

2.2 PAS and RDB-PAS measurements

A 100–150-mg (depending on the apparent bulk density of a sample) portion of a powder sample loaded on a stainless steel sample holder (standard sample thickness: 1.0 mm) was placed in a laboratory-made PAS cell (upper and bottom parts made of aluminum and stainless steel, respectively) equipped with a microphone (Knowles Electronics SP0103NC3-3 electret condenser microphone) and a Pyrex window on the upper part.

For PAS measurements to estimate the bandgap of samples [24], the PAS cell was tightly sealed and placed in a glove box (Unico UN650F) under a nitrogen atmosphere, and a monochromatic light beam from a xenon lamp (Spectral Products ASB-XE-175 xenon light source) with a grating monochromator (Spectral Products CM110) modulated at 80 Hz by a light chopper (NF Corporation 5584A) was irradiated from the top of the cell with wavelength scanning from 650 nm to 350 nm. The PA signal was detected using a digital lock-in amplifier (NF Corporation LI5630) and calibrated with spectral response with a graphite sample, absorbing the whole range of irradiated light, to compensate wavelength-dependent monochromatic light intensity. The conduction-band bottom (CBB)

position (E_{CBB}) was estimated as a function of energy from the valence-band top (VBT) from the onset wavelength (λ_{bg}) of a PAS spectrum using the equation E_{CBB} (/eV) = 1240 / (λ_{bg}/nm).

In the RDB-PAS measurements, ambient-temperature methanol-saturated argon gas was passed (ca. 30 mL min^{-1}) through a sample-loaded PAS cell in a nitrogen-filled glove box for at least 30 min. and the cell was tightly closed. Methanol was used for scavenging positive holes left by photoexcitation of VB electrons to ETs. Two light beams were combined and introduced to the PAS cell using a UV quartz combiner light guide (Moritex MWS5-1000S-UV3); one is a probe light beam from a 625-nm light-emitting diode (LED; Luxeon LXHL-ND98) intensity-modulated (80 Hz) by a digital function generator (NF Corporation DF-1906) and the other is wavelength-scanned continuous monochromatic light from the xenon lamp-monochromator used in PAS measurement, as depicted in **Fig. 1**.

(**Fig. 1** Schematic diagram and principle of RDB-PAS measurement.)

The PA signal was recorded similarly to the above-mentioned PAS measurement by scanning the continuous-light wavelength from 650 nm to 350 nm with a 5-nm step. Standard waiting and acquisition times at each wavelength were 255 s and 20 s, respectively. The observed signal intensity was plotted against energy of continuous light, and the RDB-PA spectrum was differentiated from the lower energy side to higher energy side. The obtained value was converted into ET density in the unit of μmol g^{-1} eV^{-1} with the conversion coefficient determined for each cell (See ***Section 3.2***.). The thus-obtained ERDT was a function of energy from the VBT and was replotted as a bar graph with a pitch of 0.05 eV [25,26].

3. Results and Discussion

3.1 ERDT pattern obtained by RDB-PAS

Figure 2 shows representative results of RDB-PAS measurement.

(**Fig. 2** (a) PA spectrum, (b) RDB-PA spectrum and (c) differentiated spectrum of (b) for JRC-TIO-1.)

By scanning the wavelength of continuous light from longer wavelength to shorter wavelength, PA signal intensity, i.e., photoabsorption of a sample at 625 nm, was first gradually and then steeply increased and was saturated at ca. 350 nm (**Fig. 2(b)**), indicating that electrons had accumulated in ETs from the deeper (lower energy) side to the shallower (higher energy) side, resulting in photoabsorption in the visible region (450–650 nm) as has been observed for electron-accumulated titania powders measured by DB-PAS [24]. Such saturation of PA-signal intensity at ca. 3.5 eV was commonly observed for all of the titania samples used in study. This suggests that under appropriate measurement conditions with a sufficiently long waiting time, all of the ETs were filled with electrons

and there was no accumulation of electrons in the CB. Since the RDB-PA spectrum (**Fig. 2(b)**) corresponds to the integrated form of energy distribution of ETs, ERDT, the spectrum was differentiated from the lower energy side and an ERDT pattern was obtained as shown in **Fig. 2(c)**. The scale in absolute ET density in the unit of μmol g^{-1} eV^{-1} was determined by comparison with ERDT patterns obtained by the PC method described in **Section 3.2**.

In order to avoid possible VB–ET transition by the intensity-modulated light and photoabsorption by peroxide species in the wavelength region of ca. 400–500 nm, a 625-nm red LED was chosen. As shown in a conventional PA spectrum (**Fig. 2(a)**), absorption of visible light by titania is negligible, indicating that the photoabsorption coefficient of VB–ET transition is negligibly low due to the very low density of ETs. Consequently, it is practically impossible to measure the VB–ET photoabsorption itself by conventional photoabsorption spectroscopy. However, since the VB–ET photoabsorption coefficient is not zero, i.e., at least appreciable, long-time irradiation in the presence of a strong electron donor enables accumulation of electrons in ETs; PA signal intensity saturated at ca. 350 nm (3.5 eV) was lowered when waiting time before data acquisition at each wavelength was shortened from the standard condition, 255 s, and almost no PA-signal increase was observed in the absence of methanol in the atmosphere.

Another support for the above-mentioned electron accumulation in ETs was the effect of platinum (Pt) loading; almost no increase in PA-signal intensity was observed when Pt nanoparticles were photodeposited on the titania powder (data not shown). This phenomenon is accounted for by the efficient electron transfer from electron-filled ETs in titania to Pt and possible hydrogen evolution on the Pt surface (Overall, methanol dehydrogenation proceeds slowly under visible-light irradiation.). In other words, such highly efficient electron transfer by the surface-deposited Pt, scavenging almost all of the electrons in ETs, suggests that those ETs are located predominantly on the surface or within a distance for possible electron transfer to Pt. The location of ETs will be discussed later.

When the depth of the sample holder, i.e., sample thickness, was reduced from the standard, 1 mm, saturation of PA-signal intensity at ca. 3.5 eV was appreciably lowered when the depth was less than 0.5 mm. This means that the upper 0.5-mm part of the sample contributes to the PA signal and thereby a sample layer of 1 mm in thickness may be sufficient for obtaining reproducible results.

3.2 Comparison of ERDT patterns measured by RDB-PAS and PC methods

Figure 3 is a replot of data reported previously [25].

(**Fig. 3** Comparison of ERDT patterns for JRC-TIO-2 and Ishihara Sangyo CR-EL measured by RDB-PAS (bars) and the PC method (open circles).)

Each of the anatase (Catalysis Society of Japan Reference Titania JRC-TIO-2) and rutile (Ishihara Sangyo CR-EL) titania samples exhibited a similar ERDT pattern when compared

with that measured by the PC method, though TIO-2 and CR-EL patterns obtained by RDB-PAS seemed to be slightly shifted to the upper (higher) energy side by ca. 0.2 and 0.1 eV, respectively. It should be noted that the CBB positions of anatase and rutile titanias were determined in different ways depending on the measurement methods; reported data [28] and bandgap measured by PAS [25] were used in the PC method and RDB-PAS, respectively. This may cause the different energy scales in ERDT patterns, and this is discussed later. The shapes of ERDT patterns were, however, similar for anatase and rutile samples, indicating that both methods for ERDT analysis measure the same, though the energy resolution in RDB-PAS was much higher than that in the PC method. Since the absolute molar amount (or density = μmol g^{-1}) can be determined by the PC method, the above-mentioned similarity in the pattern shapes suggests that PA-signal intensity is proportional to the density of ETs in titania samples (as reported previously [27] for total ET density) and the photoabsorption coefficient of electron-filled ETs at 625 nm is constant regardless of their energy. So far, no experimental results have been reported for photoabsorption spectra of electron-filled ETs depending on their energy (The absorption of titania samples with all of the ETs filled with electrons has been reported to be nearly structureless [24]. In the present PDB-PAS, the use of wavelength-scanned modulated light enables measurement of the spectra of electron-filled ETs with different ET energies, and this modified RDB-PAS will be reported in the future.). In other words, RDB-PAS gives ERDT patterns with relative ET density, and the density can be calibrated with the absolute density of ETs measured by the PC method.

Figure 4 shows the correlation between saturated ET density measured by the PC method and saturated PA signal intensity in the RDB-PAS analysis of the commercial titania samples.

(**Fig. 4** Correlation between total density of electron traps estimated by the PC method and saturated intensity of the RDB-PA signal. Open circles, closed circles, closed squares and open squares show anatase only, anatase-rich anatase-rutile mixture, rutile-rich anatase-rutile mixture, and rutile only samples.)

Similar to the results reported for DB-PAS measurements, in which total ET densities are measured [24], an almost linear relation could be obtained with some exceptions for samples of JRC-TIO-6 and anatase powders having very high specific surface area > 200 m^2 g^{-1} (One possible reason for the exceptions is that the power of continuous light to excite VB electrons to ETs was insufficient to fill all of the ETs with corresponding energies.). Although the reason for such deviation has not been clarified yet, the data conversion coefficient for each PA cell could be determined in the unit of mol g^{-1} eV^{-1}, and an ERDT pattern with an absolute ET density scale was obtained (**Fig. 2(c)**).

ERDT/CBB patterns could be obtained for all of the metal oxides used in previous studies including oxides of titanium, tungsten, zinc, cerium and niobium, potassium tantalate and strontium titanate, i.e., any metal oxides that have more or less ETs. In the present

setups, the shortest wavelength of continuous light and light used in PAS for determination of bandgaps was 300 nm, since a xenon arc lamp was used as a light source. Therefore, metal oxides with bandgaps larger than ca. 3.5 eV cannot be measured. Study using shorter-wavelength continuous light is now in progress to measure ERDT of wide-bandgap metal oxides.

3.3 ERDT/CBB patterns of metal-oxide powders

ERDT patterns (as **Fig. 2(c)**) obtained by differentiation of apparent RDB-PA signal spectra (**Fig. 2(b)**) were replotted in bar graphs with a pitch of 0.05 eV for comparison of them. Representative ERDT/CBB patterns of commercial titania samples are shown in **Fig. 5**.

(**Fig. 5** Representative ERDT/CBB patterns of anatase, rutile and mixed phase titania powders. Each bar shows subtotal ET density in the 0.05-eV energy range.)

The CBB position with reference to the VBT position is also shown in the graphs, and figures in brackets "< >" show the total ET density. As reported previously [25], total ET density and the CBB position predominantly depend on the specific surface area of samples and the main crystalline phase, respectively; the total ET density was nearly proportional to the corresponding surface area, and the CBB appeared at 3.2 eV, 3.0 eV and the energy range between them for anatase, rutile and their mixed samples, respectively. Therefore, these two parameters reflect bulk (surface) size and bulk structure, respectively. On the other hand, even if samples have similar specific surface areas and the same crystalline phase, ERDT patterns are not always similar (See, e.g., TIO-1 and ST-157 in **Fig. 5**.). Such a difference in ERDT is attributable to the surface structure, not reflected by the total ET density nor CBB, and ERDT/CBB patterns with total ET density may contain all of the parameters characterizing metal-oxide powders: surface structure, bulk structure and bulk (surface) size. In order to compare ERDT/CBB patterns quantitatively, the degree of coincidence of ERDT/CBB patterns (ζ; $0 < \zeta < 1$), as a weighted product of degrees of (a) ERDT pattern matching, (b) total ET density and (c) CBB position, was proposed [25,26]. Three powder samples collected from close positions in a container of Showa Denko FP-6 gave $\zeta > 0.88$, while ζ for a pair of Evonik P25 and JRC-TIO-4, the latter of which is known to be P25 provided by the Catalysis Society of Japan, was relatively high (ca. 0.7), but lower than 0.8, indicating that ζ is a good measure for identicalness, and there are appreciable differences, especially in the surface structure, due to difference in production batches and/or storage conditions even if their code name is the same [25,26].

3.4 Relative CBB and VBT positions of anatase and rutile samples

As shown in **Figs. 3 and 5**, some of the ETs had energy higher than the CBB for all of the titania samples used, and the other metal-oxide samples also showed a similar trend.

One possible reason for these curious trends is overestimation of ET energy, which might be unavoidable. It is easily expected that the photoabsorption coefficient of VB–ET transition is very small on the basis of the fact that practically no photoabsorption corresponding to VB–ET transition is observed in ordinary photoabsorption spectroscopy such as PAS. Therefore, VB–ET photoexcitation may occur from the higher DOS (density of states) part of the VB (h-DOS(VB)), not the VBT, and additional energy (ΔE), energy difference between the VBT and h-DOS(VB), is required for electrons to accumulate in ETs. Since ΔE cannot be determined (measured) at present and ERDT can only be plotted in reference to the VBT, ERDT may be shifted by ΔE upward (to the higher energy side). Theoretical and experimental studies on the distribution of DOS in the VB of metal-oxide samples could solve this problem. Another possible reason is that ETs measured in this study seem to be predominantly located on the surface and thereby the limitation that crystalline-bulk ETs have to be within the bandgap need not to be adopted. On the other hand, CBB positions seems to be measured precisely from the bandgap data, since bandgap energy is evaluated as an onset wavelength for bandgap photoabsorption as shown in **Fig. 2(a)**. This causes the above-mentioned trend. Furthermore, when a measured sample is a mixture of metal oxides of different CBBs (e.g., anatase–rutile mixed titania samples), the actual estimated CBB position tends to be governed by the lower CBB, i.e., smaller bandgap energy component (e.g., rutile); as shown in **Fig. 5**, a Showa Denko Ceramics ST-F4 sample exhibited a lower CBB of ca. 3.05 eV even though it was mainly composed of anatase with CBB of ca. 3.2 eV (as pure anatase samples, JRC-TIO-1 and Tayca ST-157, showed) while observed ERDT is predominantly composed of that of the anatase component. Thus, as a result of these complexed reasons, ERDT of samples seemed to appear on both sides of their CBB.

One of the significant points in RDB-PAS study is that ERDT is plotted as a function of energy from the VBT and, even if a mixture of powders with different VBTs is used, the resultant mixed ERDTs are shown as they have the same VBTs. **Figure 6** shows ERDT/CBB patterns of JRC-TIO-1 (anatase), TIO-3 (rutile) and their 50/50 mixture ("T1T3") prepared by just physical mixing.

(**Fig. 6** ERDT/CBB patterns of JRC-TIO-1, TIO-3, their 50/50 mixture and simulation assuming a 0.22-eV negative shift of the VBT of TIO-1.)

The mixture exhibited characteristics in its XRD pattern and specific surface area as an average of two components, suggesting the mixture is just a powder mixture. However, the ERDT pattern of T1T3 was not a simple summation of ERDTs of those components, e.g., ETs of energy > 3.3 eV, which was observed for TIO-1, could not be found. Actually, ζ between the ERDT/CBB pattern of T1T3 and a pattern synthesized by 50/50 summation of patterns of TIO-1 and TIO-3 (Estimated CBB position of T1T3 was used.) was lower than 0.35. A possible reason for this discrepancy of mixed ERDT patterns is the difference in VBT positions depending on the samples, i.e., the VBT position may be different even if the same

titania or same anatase samples are compared. Then, assuming that the VBT of TIO-1 was lower than that of TIO-3, simulation was performed by shifting the original ERDT pattern to the lower energy side with a pitch of 0.01 eV, and ζ with the T1T3 pattern was calculated. As a result, the highest ζ(a) of 0.686 (The degree of coincidence of total ET density (ζ(b) = 0.798) led to relatively low overall ζ.), which is comparably high for the pair of titania samples with the same code name, was obtained when the TIO-1 ERDT pattern was shifted by 0.22 eV. This suggests that the actual VBT position of TIO-1 is lower than that of TIO-3 by 0.22 eV. Although, generally speaking, VBTs of metal oxides have been presumed to be almost the same, not depending on the kind of metal cations, as reported previously [29] and anatase and rutile have almost the same VBT positions as suggested previously [28], the VBT (or h-DOS(VB)) of a given sample may be different sample by sample. Of course, it is impossible to exclude the possibility of interparticle electron transfer to modify the mixed ERDT, but such a sample-dependent VBT difference seems reasonable since recent papers showed that the anatase VBT was lower than the rutile VBT based on theoretical calculation and X-ray photoelectron spectroscopy (XPS) analysis [30] and based on electrochemical impedance analysis [31].

Based on these results, ERDT/CBB analysis can be used for estimation of VBT positions of metal-oxide samples, as well as CBB positions, using a standard with known VBT by the above-shown comparison and simulation of ERDT patterns. A preliminary study showed that VBT positions were not constant even for anatase (or rutile) samples and that the high-energy shift of ERDT measured by RDB-PAS compared with the PC method can be reasonably interpreted by the thus-estimated VBT (or h-DOS(VB)) positions [32].

4. Conclusions

ERDT, energy-resolved distribution of electron traps, has been successfully measured for various metal-oxide powder samples by newly developed RDB-PAS, reversed double-beam photoacoustic spectroscopy, as a sole technology for instrumental ERDT measurement, in which VB electrons are directly excited to ETs and accumulated there. The energy resolution was higher and time for data acquisition was shorter than those of the reported PC method, a conventional chemical titration method. For all of the metal-oxide samples used in this study, ERDT patterns were obtained and total amounts of ETs tended to increase with an increase in their specific surface area, at least for titania samples. Although the absolute density of ETs for samples other than titania powder samples has not yet been determined and thereby the total ET density was a relative value, the results suggest that metal oxides have more or less ETs regardless of their bulk composition, and the ETs are located predominantly on the surfaces of particles. While metal oxides tend to exhibit n-type-semiconductor properties, i.e., to have donor levels, attributable to the possible presence of oxygen vacancy in the bulk, those donor levels may scarcely account for ETs

measured by RDB-PAS, and surface reconstruction structures with unsaturated oxygen anion coordination may be the origin of the observed ETs. Theoretical studies will prove this hypothesis and the results will be reported in the future.

In the present ERDT analyses, the energies of ETs and the CBB were measured with reference to the VBT energy. For all of the measured metal-oxide power samples, shallow ETs, i.e., ETs of relatively higher energy, were distributed around their CBB positions and some of them had energy higher than the CBB. Although ET energy higher than the CBB seems strange based on the band-structure electron-energy model for semiconductors, the observed ETs are mainly on the surface, not in crystalline bulk, and they can thus have energy higher than the CBB. In addition to this, experimental limitation might induce the shift of ERDT; since it is presumed that DOS at the highest end of the VB (VBT) must be low or negligible and therefore actual excitation of VB electrons to ETs in the RDB-PAS measurements may occur from states that are slightly lower than the VBT, the energy required for VB–ET electronic transition was overestimated, when VBT–ET is assumed, resulting in higher energy ERDT. The energy correction for this overestimation, as well as the difference in VBT energies of anatase and rutile samples as mentioned below, will be reported elsewhere on the basis of results of VB energy determination by X-ray photoelectron spectroscopy under atmospheric pressure [32].

The ERDT pattern of a mixture of powders composed of almost pure anatase and rutile crystallites was not a simple summation of the ERDT patterns of the components, but the pattern of the mixture was reproduced well by simulation with the assumption that the VBT of one of the samples is different from that of the other, i.e., summation of two patterns with some shift of a pattern. For a given combination of anatase and rutile samples, a ca. +0.2-eV lower shift of the anatase VBT led to a reasonable fit of the simulated pattern with the observed pattern for the mixture. It is thus suggested that the VBT position of a given sample can be estimated by comparison of the ERDT patterns of the sample alone and a mixture with an appropriate standard the VBT position of which has been measured/reported.

In conclusion, the newly developed RDB-PAS enables not only measurement of ERDT/CBB patterns of metal-oxide powder samples, as a fingerprint for identification and detailed characterization [25,26], but also estimation of the VBT (or h-DOS(VB)) position. The thus-reported ERDTs may reflect significant properties that are closely related to the electrochemical functionality of metal-oxide materials, which have remained less characterized for their surfaces as an interface of charge transfer, and thereby this analytical method will, at least, provide basic information on photoelectrochemical and photocatalytic properties of electrodes and powders, respectively, composed of metal-oxide particles. Further improvements of energy resolution, measurable energy range and acquisition time are now in progress and will be reported elsewhere.

Acknowledgements

The authors thank Professor Taro Toyoda (The University of Electro-Communications) and the staff in the Technical Division of Institute for Catalysis (Hokkaido University) for basic design of PAS setups and construction of the apparatuses, respectively.

References

[1] B. Ohtani, Revisiting the fundamental physical chemistry in heterogeneous photocatalysis: its thermodynamics and kinetics, Phys. Chem. Chem. Phys. 16 (2014) 1788–1797.

[2] S. Kawaguchi, S. Hasegawa, K. Kaseda, S. Kurita, Studies on the surface electron traps in photoconductors (I) DPPH method and hammett method, Denshi Shashin 8 (1968) 92–100 (in Japanese).

[3] A. K. Ghosh, F. G. Wakim, R. R. Addiss, Jr., Photoelectronic processes in rutile, Phys. Rev. 184 (1969) 979–988.

[4] Y. Inoue, S. Hasegawa, T. Kawaguchi, Surface properties and catalytic function of a few metal oxides, Nippon Kagaku Zasshi 91 (1970) 1034–1038 (in Japanese)

[5] S. Hasegawa, T. Kawaguchi, Surface properties and photoconductivity of hydrogen-reduced titanium(IV) oxide, Nippon Kagaku Zasshi 92 (1971) 389–392 (in Japanese).

[6] U. Kölle, J. Moser, M. Grätzel, Dynamics of interfacial charge-transfer reactions in semiconductor dispersions. Reduction of cobaltoceniumdicarboxylate in colloidal TiO_2, Inorg. Chem. 24 (1985) 2253–2258.

[7] R. F. Howe, M. Grätzel, EPR observation of trapped electrons in colloidal TiO_2, J. Phys. Chem. 89 (1985) 4495–4499.

[8] B. Ohtani, T. Atsumi, S.-i. Nishimoto, T. Kagiya, Multiple-mode responsive device. Photo- and electro-chromic composite thin film of tungsten oxide with titanium oxide, Chem. Lett. 17 (1988) 295–298.

[9] S. Ikeda, N. Sugiyama, S.-y. Murakami, H. Kominami, Y. Kera, H. Noguchi, K. Uosaki, T. Torimoto, B. Ohtani, Quantitative analysis of defective sites in titanium(IV) oxide photocatalyst powders, Phys. Chem. Chem. Phys. 5 (2003) 778–783.

[10] B. Ohtani, Y. Ogawa, S.-i. Nishimoto, Photocatalytic activity of amorphous-anatase mixture of titanium(iv) oxide particles suspended in aqueous solutions, J. Phys. Chem. B 101 (1997) 3746-3752.

[11] Y. Shiraishi, H. Hirakawa, Y. Togawa, Y. Sugano, S. Ichikawa, T. Hirai, Rutile crystallites isolated from degussa (Evonik) P25 TiO_2: highly efficient photocatalyst for chemoselective hydrogenation of nitroaromatics, ACS Catal. 3 (2013) 2318–2326.

[12] Y. Shiraishi, H. Hirakawa, Y. Togawa, T. Hirai, Noble-metal-free deoxygenation of epoxides: titanium dioxide as a photocatalytically regenerable electron-transfer catalyst, ACS Catal. 4 (2014) 1642–1649.

[13] D. V. Lang, Deep-level transient spectroscopy: a new method to characterize traps in semiconductors, J. Appl. Phys. 45 (1974) 3023–3032.

[14] T. Miyagi, T. Ogawa, M. Kamei, Y. Wada, T. Mitsuhashi, A. Yamazaki, E. Ohta, T. Sato, Deep level transient spectroscopy analysis of an anatase epitaxial film grown by metal organic chemical vapor deposition, Jpn. J. Appl. Phys. 40 (2001) L404–L406.

[15] T. Miyagi, M. Kamei, I. Sakaguchi, T. Mitsuhashi, A. Yamazaki, Photocatalytic property and deep levels of nb-doped anatase TiO_2 film grown by metalorganic chemical vapor depostion, Jpn. J. Appl. Phys. 43 (2004) 775–776.

[16] M. Buchalska, M. Kobielusz, A. Matuszek, M. Pacia, S. Wojtyła, W. Macyk, On oxygen activation at rutile- and anatase-TiO_2, ACS Catal. 5 (2015) 7424–7431.

[17] A. G. Bell, On the production and reproduction of sound by light, Am. J. Sci. 20 (1880) 305–324.

[18] A. Rosencwaig, A. Gersho, Theory of the photoacoustic effect with solids, J. Appl. Phys. 47 (1976) 64–69.

[19] T. Toyoda, S. Shimamoto, Effects of Bi_2O_3 impurities in ceramic ZnO on photoacoustic spectra and current-voltage characteristics, Jpn. J. Appl. Phys. 37 (1998) 2827–2831.

[20] T. Toyoda, H. Kawano, Q. Shen, A. Kotera, M. Ohmori, Characterization of electronic states of tio_2 powders by photoacoustic spectroscopy, Jpn. J. Appl. Phys. 39 (2000) 3160–3163.

[21] T. Toyoda, I. Tsuboya, Apparent band-gap energies of mixed TiO_2 nanocrystals with anatase and rutile structures characterized with photoacoustic spectroscopy, Rev. Sci. Instrum. 74 (2003) 782–784.

[22] N. Murakami, O.-O. Prieto-Mahaney, T. Torimoto, B. Ohtani, Photoacoustic spectroscopic analysis of photoinduced change in absorption of titanium(IV) oxide photocatalyst powders: a novel feasible technique for measurement of defect density, Chem. Phys. Lett. 426 (2006) 204–208.

[23] N. Murakami, R. Abe, O.-O. Prieto-Mahaney, T. Torimoto, B. Ohtani, Photoacoustic spectroscopic estimation of electron mobility in titanium(IV) oxide photocatalysts, Stud. Surf. Sci. Catal. 172 (2007) 429–432.

[24] N. Murakami, O.-O. Prieto-Mahaney, R. Abe, T. Torimoto, B. Ohtani, Double-beam photoacoustic spectroscopic studies on transient absorption of titanium(IV) oxide photocatalyst powders, J. Phys. Chem. C 111 (2007) 11927–11935.

[25] A. Nitta, M. Takase, M. Takashima, N. Murakami, B. Ohtani, A fingerprint of metal-oxide powders: energy-resolved distribution of electron traps, Chem. Commun. 52 (2016) 12096–12099.

[26] A. Nitta, M. Takashima, M. Takase, B. Ohtani, Catal. Today, in press, 10.1016/j.cattod.2017.12.020.

[27] B. Ohtani, O.-O. Prieto-Mahaney, F. Amano, N. Murakami, R. Abe, What are titania photocatalysts?—An exploratory correlation of photocatalytic activity with structural and physical properties, J. Adv. Oxid. Technol. 13 (2010) 247–261.

[28] L. Kavan, M. Grätzel, S. E. Gilbert, C. Klemenz, J. Scheel, Electrochemical and photoelectrochemical investigation of single-crystal anatase, J. Am. Chem. Soc. 118 (1996) 6716–6723.

[29] D. E. Scaife, Oxide semiconductors in photoelectrochemical conversion of solar energy, Sol. Energy 25 (1980) 41–54.

[30] D. O. Scanlon, C. W. Dunnill, J. Buckeridge, S. A. Shevlin, A. J. Logsdail, S. M. Woodley, C. R. A. Catlow, M. J. Powell, R. G. Palgrave, I. P. Parkin, G. W. Watson, T. W. Keal, P. Sherwood, A. Walsh, A. A. Sokol, Band alignment of rutile and anatase TiO_2, Nat. Mater. 12 (2013) 798–801.

[31] D. Zhang, M. Yang, H. Gao, S. Dong, Translating XPS measurement procedure for band alignment into reliable ab initio calculation method, J. Phys. Chem. C, 121 (2017) 7139–7143.

[32] A. Nitta, M. Takashima, Y. Murakami, B. Ohtani, Estimation of valence band-top positions of anatase and rutile particles through reversed double-beam photoacoustic spectroscopy, Chem. Phys. Lett. (2017) (in preparation).

Table 1 Structural and ET-related properties and photocatalytic-activity rank of titania samples used in this study.

supplier[a]	code	composition[b] (%)		SSA[c]/	D[d]/μmol	E_{CBB}[e]/e	activity rank[f]		
		anatase	rutile	$m^2\ g^{-1}$	g^{-1}	V	H_2	CO_2	O_2
CSJ	TIO-1	91	0	79	97	3.20	42	34	33
CSJ	TIO-2	91	0	17	32	3.14	48	37	28
CSJ	TIO-3	0	90	47	98	2.98	44	48	32
CSJ	TIO-4	72	23	53	129	3.06	6	2	16
CSJ	TIO-6	0	78	102	152	3.03	41	36	49
Aerosil	P25	82	15	58	114	3.06	16	8	14
ISK	CR-EL	1	94	8	23	2.97	7	42	4
SDC	ST-F4	77	14	52	152	3.05	35	4	19
SDC	FP-6	83	8	104	154	3.15	33	9	24
SDC	ST-G2	3	95	4	29	2.95	1	43	6
Tayca	ST-157	81	0	81	75	3.20	49	41	41

[a]CSJ: Catalysis Society of Japan, Aerosil: Nippon Aerosil, ISK: Ishihara Sangyo, SDC: Showa Denko Ceramics, and Tayca: Tayca Corporation. [b]The rest corresponds to non-crystalline component. [c]Specific surface area. [d]Total density of ETs. [e]CBB position. [f]Rank of photocatalytic activities among 49 titania samples in (H_2) methanol dehydrogenation, (CO_2) oxidative decomposition of acetic acid in aerobic aqueous solutions and (O_2) oxygen evolution from deaerated aqueous silver fluoride solutions [25].

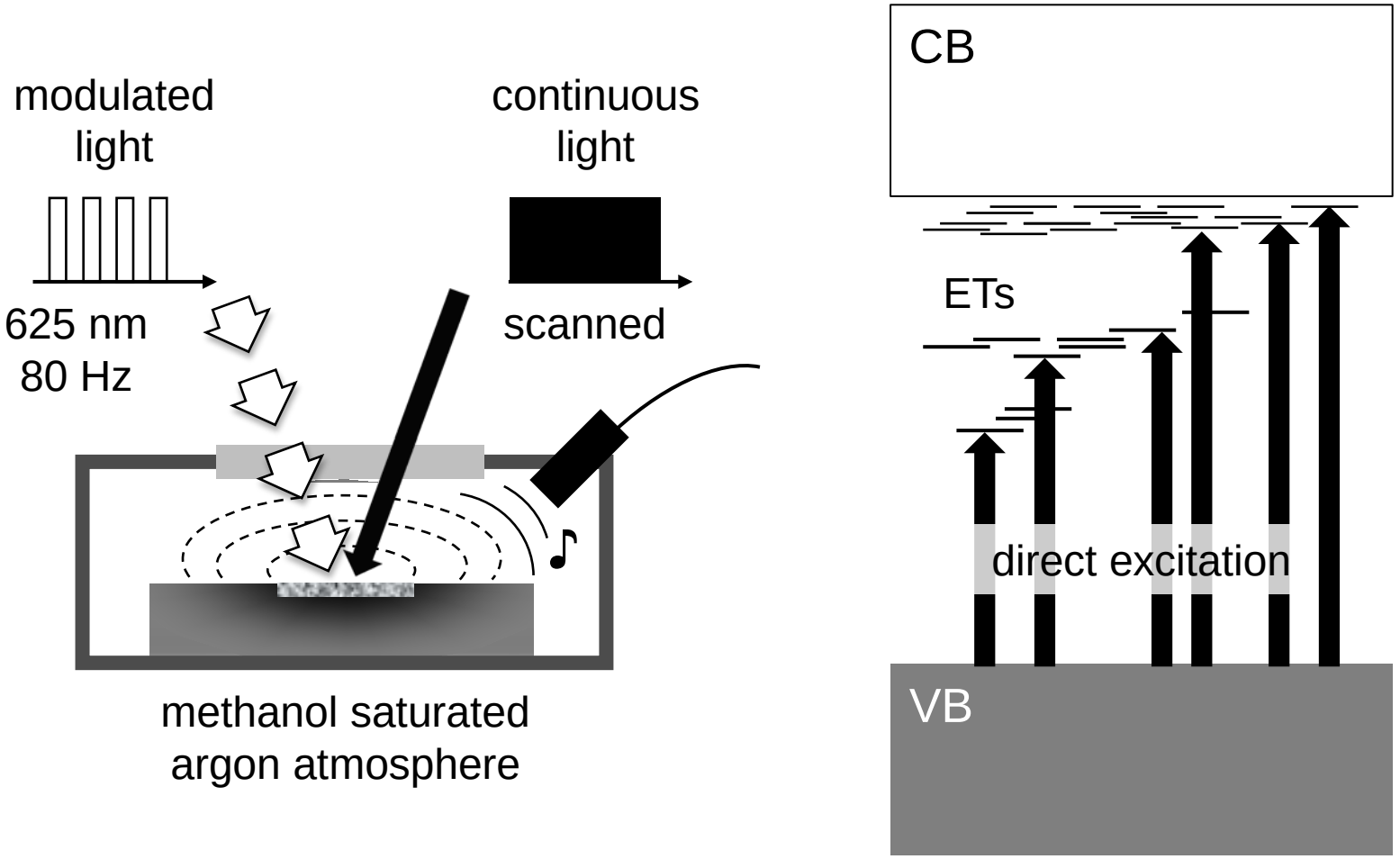
modulated
light
continuous
light
625 nm
80 Hz
scanned
methanol saturated
argon atmosphere
CB
ETs
direct excitation
VB

Fig. 1

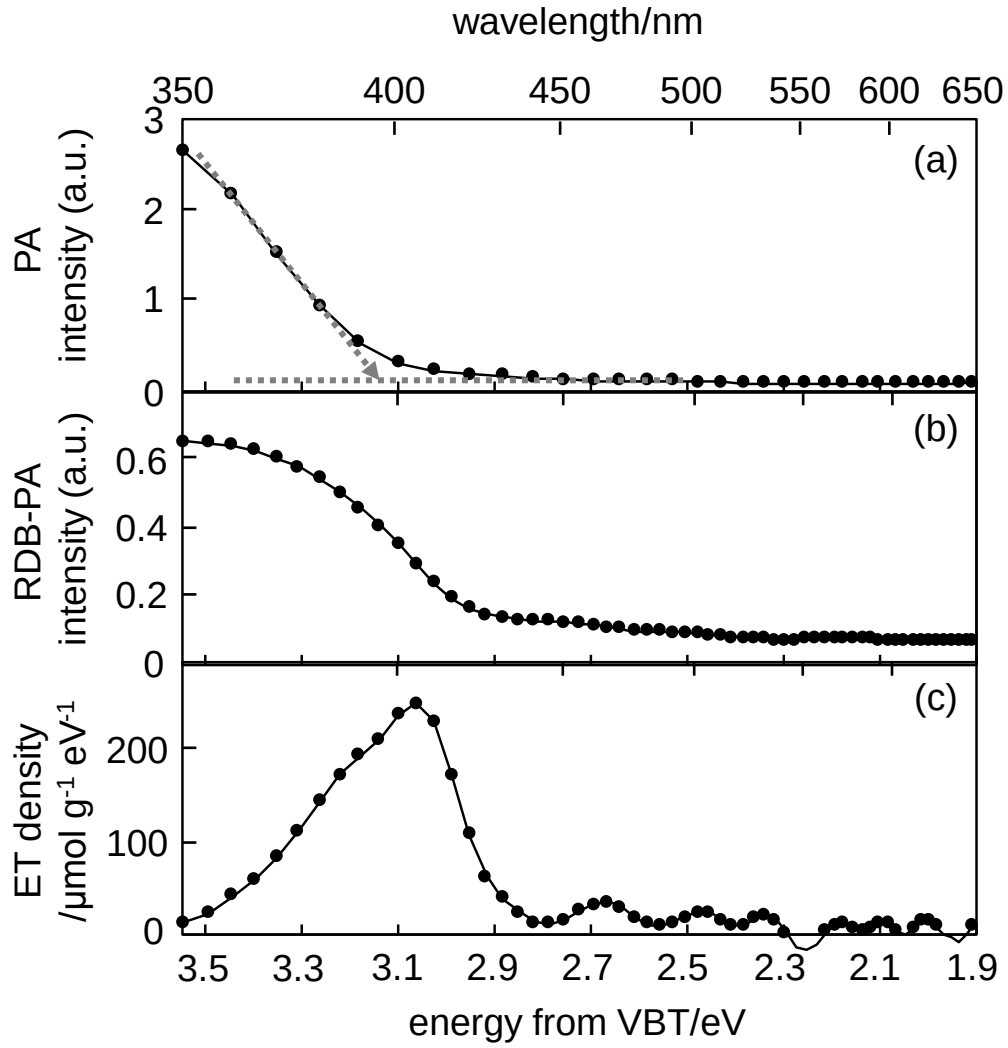
wavelength/nm
350
400
450
500
550
600
650
PA
intensity (a.u.)
3
2
1
0
(a)
RDB-PA
intensity (a.u.)
0.6
0.4
0.2
0
(b)
ET density
/μmol g-1 eV-1
200
100
0
(c)
3.5
3.3
3.1
2.9
2.7
2.5
2.3
2.1
1.9
energy from VBT/eV

Fig. 2

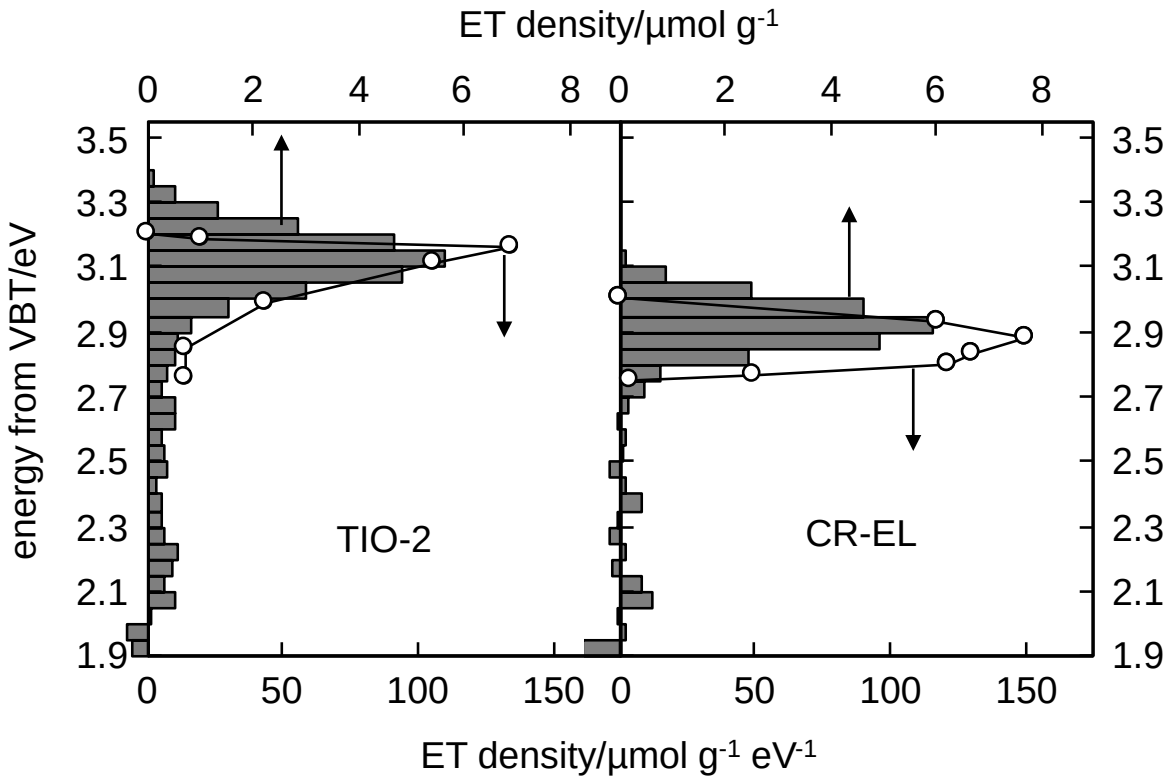
ET density/µmol g-1
0
2
4
6
8
3.5
3.3
3.1
2.9
2.7
2.5
2.3
2.1
1.9
energy from VBT/eV
TIO-2
CR-EL
0
50
100
150
ET density/µmol g-1 eV-1

Fig. 3

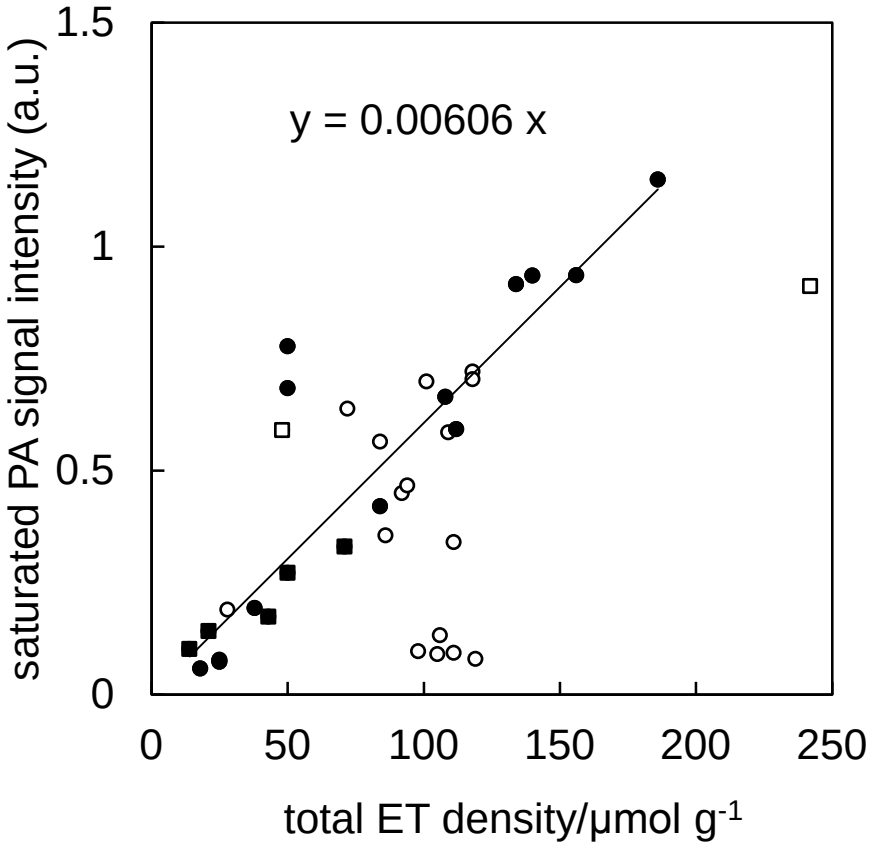
y = 0.00606 x
saturated PA signal intensity (a.u.)
total ET density/μmol g-1
0
0.5
1
1.5
0
50
100
150
200
250

Fig. 4

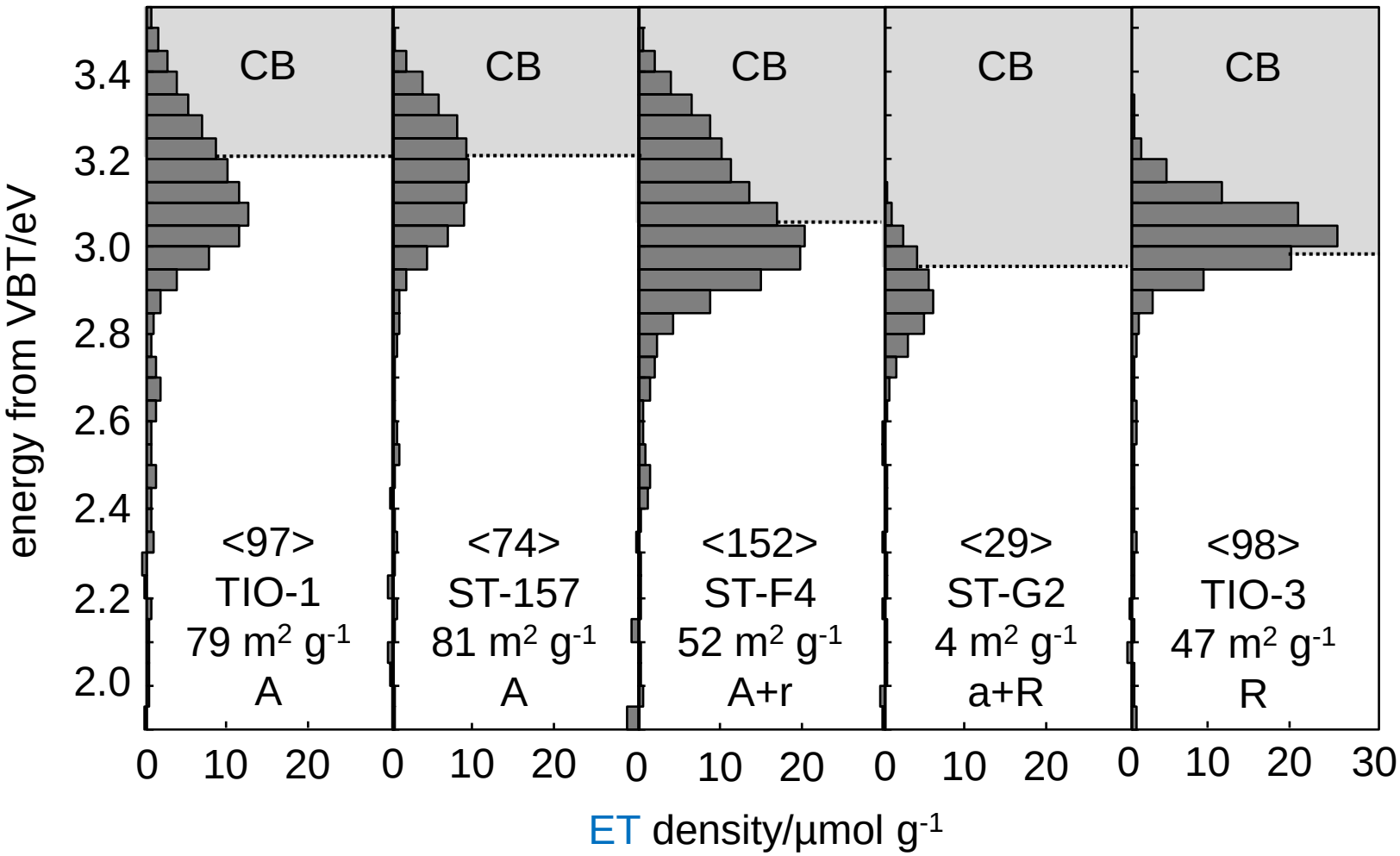
energy from VBT/eV
3.4
3.2
3.0
2.8
2.6
2.4
2.2
2.0
CB
CB
CB
CB
CB
<97>
TIO-1
79 m² g⁻¹
A
<74>
ST-157
81 m² g⁻¹
A
<152>
ST-F4
52 m² g⁻¹
A+r
<29>
ST-G2
4 m² g⁻¹
a+R
<98>
TIO-3
47 m² g⁻¹
R
0 10 20 0 10 20 0 10 20 0 10 20 0 10 20 30
ET density/μmol g⁻¹

Fig. 5

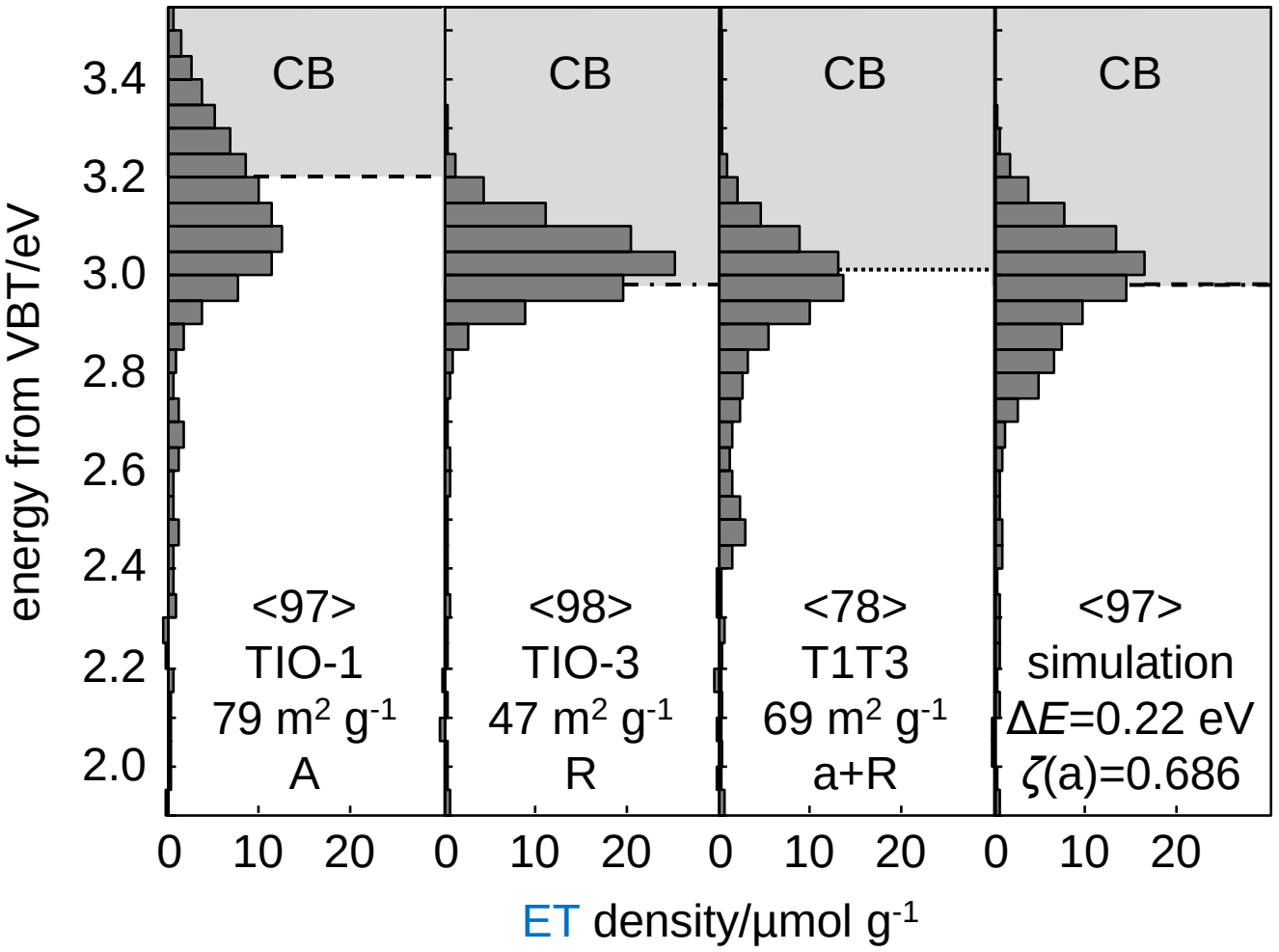
energy from VBT/eV
3.4
3.2
3.0
2.8
2.6
2.4
2.2
2.0
CB
CB
CB
CB
<97>
TIO-1
79 m² g⁻¹
A
<98>
TIO-3
47 m² g⁻¹
R
<78>
T1T3
69 m² g⁻¹
a+R
<97>
simulation
ΔE=0.22 eV
ζ(a)=0.686
0 10 20
0 10 20
0 10 20
0 10 20
ET density/μmol g⁻¹

Fig. 6